ORIGINAL ARTICLE

Suppressing Wnt signaling of the blood−tumor barrier to intensify drug delivery and inhibit lipogenesis of brain metastases

Yang Tong[a,†], Pei An[a,†], Puxian Tang[a], Rui Mu[a], Yuteng Zeng[a], Hang Sun[a], Mei Zhao[a], Ziyan Lv[a], Pan Wang[a], Wanjun Han[a], Chunshan Gui[a], Xuechu Zhen[a,b], Liang Han[a,b,*]

[a]*Jiangsu Key Laboratory of Neuropsychiatric Diseases and College of Pharmaceutical Sciences, Soochow University, Suzhou 215123, China*
[b]*Jiangsu Province Engineering Research Center of Precision Diagnostics and Therapeutics Development, Soochow University, Suzhou 215123, China*

Abstract Lipogenesis is often highly upregulated in breast cancer brain metastases to adapt to intracranial low lipid microenvironments. Lipase inhibitors hold therapeutic potential but their intra-tumoral distribution is often blocked by the blood−tumor barrier (BTB). BTB activates its Wnt signaling to maintain barrier properties, *e.g.*, Mfsd2a-mediated BTB low transcytosis. Here, we reported VCAM-1-targeting nano-wogonin (W@V-NPs) as an adjuvant of nano-orlistat (O@V-NPs) to intensify drug delivery and inhibit lipogenesis of brain metastases. W@V-NPs were proven to be able to inactivate BTB Wnt signaling, downregulate BTB Mfsd2a, accelerate BTB vesicular transport, and enhance tumor accumulation of O@V-NPs. With the ability to specifically kill cancer cells in a lipid-deprived environment with IC_{50} at 48 ng/mL, W@V-NPs plus O@V-NPs inhibited the progression of brain metastases with prolonged survival of model mice. The combination did not induce brain edema, cognitive impairment, and systemic toxicity in healthy mice. Targeting Wnt signaling could safely modulate the BTB to improve drug delivery and metabolic therapy against brain metastases.

1. Introduction

Metastatic dissemination from solid tumors remains a formidable clinical challenge and contributes to cancer-related mortality[1]. In particular, brain metastases are associated with high incidence and poor survival outcomes owing to the advances in treatments of solid tumors, earlier diagnosis, and limited therapeutic options for brain metastases[2-4]. Due to the characteristics of highly intracranial dispersion, it is urgent to develop efficient pharmacological therapy for brain metastases. However, brain metastases are often refractory to therapies that control primary tumors at extracranial sites, which could be ascribed to multiple factors[2-5]. Accumulating evidence suggests that both the blood−brain barrier (BBB)/blood−tumor barrier (BTB) and the brain tumor microenvironment contribute to resistance and challenges associated with treating cancers in this tissue site[1].

The BBB/BTB blocks most entry of blood substances into the brain's extracellular fluid[6,7], creating a unique brain extracellular nutrient environment. Nutrient deprivation in the brain microenvironment relative to peripheral tissues necessitates tumor metabolic adaptations to satisfy intracranial tumor growth[1,8,9]. Breast cancer brain metastases upregulate fatty acid synthase (FAS) for lipogenesis. The selective inhibitor TVB3166 was proven to defer the growth of *ex vivo* intracranial breast tumors[1], suggesting the therapeutic potential of targeting lipogenesis for brain metastases. However, the BTB also blocks drug penetration into brain metastases. Specific BTB regulation holds the potential to enhance the efficiency of targeting lipogenesis.

Endothelial Wnt signaling is essential for BBB development by regulating the expression of a series of functional proteins[10,11], *e.g.*, transcytosis-controlling Mfsd2a[12,13]. It is hyperactive in the BTB of multiple types of brain tumors, *e.g.*, glioma, medulloblastoma, and brain metastases from lung cancers and breast cancers[14-17]. BTB Wnt signaling was shown to be repressible, leading to increased drug transport and treatment responses[15]. Wnt inhibitors, *e.g.*, wogonin (WOG)[18], hold the potential to regulate the BTB for promoting specific transport across the BTB and into brain metastases.

Vascular cell adhesion molecule-1 (VCAM-1) is often highly expressed in the BTB in brain metastases[19]. Inspired by the contribution of Wnt signaling to the BTB properties[14-17], here we reported the delivery of WOG by VCAM-1-targeting nanoparticles (W@V-NPs) to regulate the Mfsd2a-controlled BTB transcytosis for improved delivery of orlistat (ORL)-loaded O@V-NPs to brain metastases and pharmacological therapy (Scheme 1). We found that different from routine anticancer drugs including doxorubicin and cisplatin, ORL possessed specific cytotoxicity to breast cancer cells in the lipid-deprived brain environment with the IC$_{50}$ difference of ∼3000-fold. W@V-NPs were shown to efficiently target BTB endothelial cells and diminish BTB Wnt signaling and Mfsd2a reversibly to boost the penetration of O@V-NPs into brain metastases. The physical combination of W@V-NPs and O@V-NPs (WO@V-NPs) produced effective therapy against breast cancer brain metastases with minimal side effects.

2. Materials and methods

2.1. Cell lines and animals

Mouse BBB endothelial cells (bEND.3) and mouse 4T1 and human MDA-MB-231 breast cancer cells were obtained from the Cell Bank of the Chinese Academy of Sciences, Shanghai, China. Brain metastatic breast cancer cells (231Br and 4T1Br) were kindly provided by Dr. Patricia Steeg at the National Cancer Institute (Maryland, USA). All cells were grown in DMEM supplemented with 10% fetal bovine serum, 100 units/mL penicillin, and 100 μg/mL streptomycin in a 37 °C incubator containing 5% CO$_2$.

Adult ICR mice (female and 20−25 g) and BALB/c immune-deficient nude mice (female and 18−20 g) were purchased from CAVENS (Changzhou) and maintained under standard housing conditions. All animal-related experiments were performed following the guidelines of the Ethics Committee for Animal Experiments and the Soochow University Institutional Animal Care and Use Committee. Mouse models of breast cancer brain metastases constructed through intracardiac injection of brain-seeking 231Br or 4T1Br cells have been well characterized to recapitulate the condition of the early stage of brain metastases and maintain the integrity of BBB contrasting to the widely adopted local intracranial injection[20-25]. The mouse model was established *via* intracardiac injection of 2.5 × 10^5 231Br (or 1 × 10^5 4T1Br cells) or intracranial injection of 2 × 10^4 4T1Br cells into BALB/c nude mice. According to previous reports[26,27], nude mice were anesthetized with chloral hydrate and firmly secured in a stereotaxic apparatus with front paws extended above the head. Brain-seeking 231Br or 4T1Br cells in 0.1 mL PBS 7.4 were loaded into a 1-mL syringe with a 26-G needle. After inserting the needle into the third intercostal space at a distance of 3 mm to the left side of the sternum with a depth of ∼6 mm, cells were injected slowly at a uniform speed over 20−30 s. Then mice were carefully checked and put back into cages. For intracranial injection of 4T1Br cells, nude mice were anesthetized with chloral hydrate and firmly secured in a stereotaxic apparatus to expose the skull and drill a hole at 2 mm to the right of the fontanel. Then brain-seeking 4T1Br cells (1 × 10^5) in 5 μL PBS 7.4 were loaded into a 10-μL micro-syringe and injected slowly at a uniform speed over 2 min into the right striatum (1.8 mm lateral to the bregma and 3 mm of depth) using the stereotactic apparatus with mouse adaptor. After needle withdrawal, the skull hole was closed with bone wax. Then mice were carefully checked and put back into cages.

2.2. Characterization of FAS and chemotherapeutic sensitivity of breast cancer brain metastases

Frozen 20-μm-thick brain sections excised from 231Br model mice (intracardiac injection method) were stained for FAS and imaged under a confocal laser scanning microscope (Nikon AIR HD25). FAS expression and activity in healthy tissues and diseased tissues from 4T1Br model mice (intracranial injection
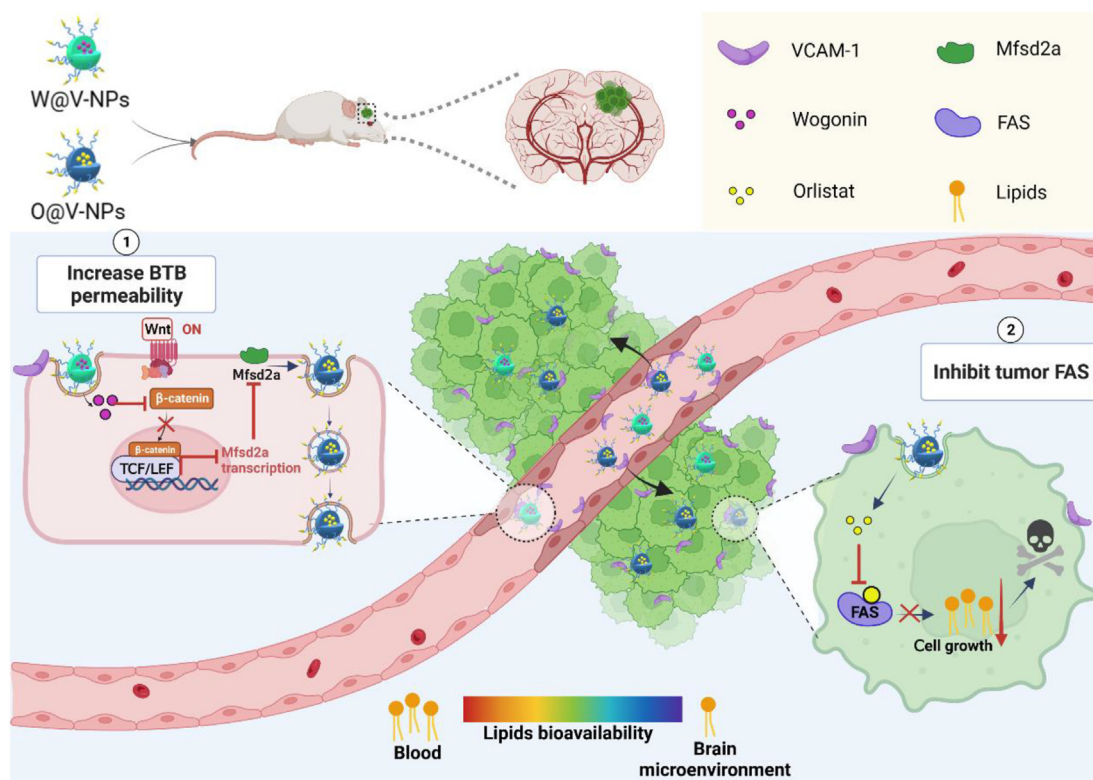
Scheme 1   The illustration shows that WO@V-NPs (the physical combination of W@V-NPs and O@V-NPs) improve transcellular transport across the BTB *via* inhibiting BTB Wnt signaling, and treat brain metastases *via* interfering tumor lipid metabolism. By targeting VCAM-1, W@V-NPs deliver and release the Wnt inhibitor WOG to BTB endothelial cells, inhibit BTB Wnt signaling, reduce BTB Mfsd2a expression, and then increase BTB transcytosis for O@V-NPs to accumulate in breast cancer brain metastases efficiently. In the premise of W@V-NPs, O@V-NPs efficiently target metastatic tumor cells and restrain tumor progression by releasing ORL and interfering with FAS-involved tumor lipid metabolism.

method) was also characterized by Western blotting and using the FAS activity assay kit (BC0550, Solarbio life sciences).

Lipid-stripped serum (−lipid) was generated to prepare a lipid-depleted medium. Briefly, fetal bovine serum was mixed with isochoric di-isopropyl ether and n-butanol mixture (5:4:1, *v/v/v*) for 30 min at room temperature. After centrifugation at $4000\times g$ for 15 min at 4 °C, phases were separated. The lower phase was collected and mixed with di-isopropyl ether (original volume of serum) for 30 min at room temperature. The lower phase was collected, stirred overnight under argon, and dialyzed against saline at 4 °C. Control serum (+lipid) was dialyzed in the same manner. The protein concentration of lipid-stripped and control sera was quantified using a Bradford Assay, corrected with saline, and stored at −20 °C. 4T1Br cells were cultured in either + lipid medium or−lipid medium for 72 h and evaluated for FAS expression and activity. 4T1Br cells were also cultured in either + lipid medium or−lipid medium for 24 h and then treated with ORL in respective mediums for another 48 h to evaluate the effect of the treatment on FAS activity.

To evaluate the chemotherapeutic sensitivity of breast cancer brain metastases, 231Br cells and 4T1Br cells in either + lipid medium or−lipid medium were treated with various drugs at different concentrations for 48 h. Cell proliferation was then quantified using methyl thiazolyl diphenyl-tetrazolium bromide assay.

2.3.   Synthesis of NPs

Poly(lactic-*co*-glycolic acid)-poly(*ε*-carbobenzoxy-L-lysine) (PLGA-PLL) was synthesized as nanoparticles (NPs) starting material *via* coupling PLGA (719900, Sigma) with PLL (P4510, Sigma) using DCC and DMAP[13,28-34]. All NPs were prepared using the ultrasonic emulsion solvent evaporation method. Typically, WOG (20 mg), ORL (20 mg), IR780 (4 mg, 6 μmol), doxorubicin (10 mg), or Dir (2 mg) was added dropwise to 100 mg PLGA−PLL in 2 mL ethyl acetate (oil phase) under vortex. This mixture was sonicated at 300 W for 30 s and added dropwise to 4 mL 2.5% polyvinyl alcohol (external aqueous phase) under vortex. The mixture was sonicated at 300 W for 30 s to form an o/w emulsion and quickly poured into a beaker containing 100 mL 0.3% polyvinyl alcohol (volatile aqueous phase) and stirred overnight to evaporate ethyl acetate. Solidified nanosuspensions were centrifuged at $70,000\times g$ for 20 min to remove polyvinyl alcohol and ultrasonically dispersed in PBS 7.4. The exposed hydrophilic PLL at the NP surface was conjugated with the *α*-malemidyl-*u-N*-hydroxysuccinimidyl polyethyleneglycol 3500 (11.2 mg, Jenkem, Beijing) for 1 h at room temperature to display polyethyleneglycol and maleimide. Then, NPs were centrifuged at $70,000\times g$ for 20 min to remove excess functional polyethyleneglycol and reacted with VCAM-1-targeting peptide (5.56 mg, 4 μmol, VHPKQHRGGSKGC, Nanjing Peptide Biotech, China) in PBS 7.4 for 1 h at room temperature *via* the reaction

between terminal maleimide and free sulfhydryl. Functionalized NPs were further reacted with excess low molecular weight methoxyl polyethyleneglycol thiol (MW 350) for 1 h at room temperature to block the remaining unreacted maleimide. NPs were centrifuged to remove excess peptide and methoxyl polyethyleneglycol thiol, suspended in H_2O, and lyophilized for storage and characterization.

2.4. Physicochemical characterization

The appearance and morphology of W@V-NPs and O@V-NPs were examined under a transmission electron microscope (JEM-2010, JEOL, Japan). Hydrodynamic diameter and Zeta potential were measured using dynamic light scattering (Zetasizer Nano ZS, Malvern). The loading efficiency for WOG and ORL was determined using HPLC (Agilent 1260, USA) with an ultraviolet detector at 275 and 205 nm. *In vitro* release of WOG and ORL was performed in 50 mL PBS of pH 7.4 or pH 5.0 with 0.5% sodium dodecyl sulfate using a dialysis bag (MWCO 3500). WOG and ORL released at various times were quantified through the above methods. 4T1Br cells in either + lipid medium or−lipid medium were treated with V-NPs and O@V-NPs for 48 h to evaluate their effects on FAS activity. To evaluate the therapeutic effect of O@V-NPs, 4T1Br cells in−lipid medium were treated with different formulations for 48 h and measured for cell proliferation.

2.5. Targeting BTB and brain metastases by specially targeting VCAM-1

To evaluate the intracranial expression of VCAM-1, 231Br model mice (intracardiac injection method) and 4T1Br model mice (intracardiac injection method) were intravenously injected with 100 μL of PE rat anti-mouse CD31 (BD Pharmingen) and perfused at 1 h post-injection for brain resection. Then 20-μm-thick frozen sections from excised brains were stained for VCAM-1 to check its expression in blood vessels in healthy brains and brain metastases.

Brain tumor conditioned medium (TCM) was prepared from 231Br or 4T1Br cell culture to induce the production of BTB endothelial cells[28]. Briefly, a complete medium was added to the tumor cell culture at 60% confluence, and after 48 h incubation was collected as TCM by 10 min centrifugation at $3000 \times g$ and 4 °C. The bEND.3 cells were incubated with TCM for 48 h to form BTB endothelial cells. The expression of VCAM-1 in BBB endothelial cells, BTB endothelial cells, MDA-MB-231 cells, 231Br cells, 4T1 cells, and 4T1Br cells was characterized by Western blotting and immunofluorescence staining.

BBB endothelial cells, BTB endothelial cells, 231Br cells, and 4T1Br cells were treated with doxorubicin-loaded NPs or V-NPs (5 μg doxorubicin/mL) for 3 h. Then cellular uptake was quantitatively measured using flow cytometry. To investigate whether V-NPs could selectively penetrate the BTB and enter brain metastatic tumor cells, an *in vitro* BBB model was established by seeding 1×10^5 cells/well bEND.3 cells into the upper insert of a 12-well Transwell plate with a 3 μm pore diameter membrane (Cat. 665630, Greiner, China). For *in vitro* BTB model, at the time of bEND.3 plating, 8×10^4 4T1Br cells/well were plated into the lower chamber. At 48 h after 4T1Br plating, the medium was changed to 4T1Br TCM for at least 48 h incubation until the transendothelial electrical resistance reached between 150 and 300 $\Omega \cdot cm^2$. Then IR780 and doxorubicin coloaded NPs and V-NPs in the control medium or 4T1Br TCM

(4 μg IR780 and 5 μg doxorubicin/mL) were added into the upper chamber. After 6 h incubation, IR780 and doxorubicin in the blood side (upper chamber), endothelial cells, brain side (lower chamber), and tumor cells were measured at 780/817 nm and 537/584 nm using a microplate reader (M1000 Pro, Tecan) for their distribution.

For semi-quantitative pharmacokinetics and biodistribution studies, both healthy ICR mice and 4T1Br model mice (intracranial injection method) were intravenously injected with IR780 (1% Tween 80), IR780-loaded NPs, V-NPs, or brain-targeted angiopep-2-modified NPs (A-NPs) at a dose of 0.75 mg IR780/kg. Twenty microliters of blood were obtained at different times through the tail vein and mixed with DMSO (180 μL) to extract and quantify IR780 using the IVIS imaging system. At 48 h, mice were perfused for excision of major organs and imaging using an IVIS imaging system. The fluorescence intensity of IR780 was semi-quantified using Living Image 3.0 and compared with standard samples to obtain blood concentration−time profiles and biodistribution data. To evaluate the pharmacokinetics and biodistribution of W@V-NPs using the quantitative LC−MS method, 4T1Br model mice were intravenously injected with W@V-NPs (5 mg WOG/kg). Then serum was collected at 2, 8, 14, 26, 50, 74, and 98 h, and major organs including intracranial metastatic tumors were harvested at 50 h for WOG measurements using LC−MS.

To study whether V-NPs could target brain metastases at the *in vivo* level, 231Br model mice (intracardiac injection method) and 4T1Br model mice (intracardiac injection method) were intravenously injected with doxorubicin-loaded NPs or V-NPs at a dose of 10 mg doxorubicin/kg after the onset of neurological symptoms. At 12 h, mice were perfused and excised brains were sectioned into 20-μm-thick frozen sections using a CM1950 cryostat (Leica Microsystems, Wetzlar, Germany). Sections for healthy brains and brain metastases were examined under a confocal laser scanning microscope.

2.6. Regulation of BTB Wnt signaling and Mfsd2a

To evaluate the status of Wnt signaling of BTB endothelial cells, the cells were stained for lymphoid enhancer-binding factor 1 (LEF1, marker of Wnt activation) and characterized using Western blotting and immunofluorescence staining. Cells treated with 20 mmol/L Wnt classic agonist LiCl (24 h) were used as a positive control of activated Wnt signaling.

To investigate the effect of Wnt signaling on the expression of Mfsd2a, bEND.3 cells were treated with LiCl at different concentrations for 24 h. To evaluate whether Wnt inhibitor WOG could regulate Mfsd2a, bEND.3 cells were preincubated with 20 mmol/L LiCl for 24 h and then treated with WOG at different concentrations for 24 h. Then cells were collected to characterize Mfsd2a using Western blotting.

To further investigate the effects of W@V-NPs on BTB Wnt signaling and Mfsd2a, BTB endothelial cells were treated with WOG (different concentrations), V-NPs, or W@V-NPs (20 μg WOG/mL) for 24 h to characterize LEF1 and Mfsd2a using Western blotting.

To study the timeliness and reversibility of Mfsd2a regulation, bEND.3 cells were treated with either cycloheximide (0.1 mg/mL) or W@V-NPs (20 μg WOG/mL) for different times. In addition, bEND.3 cells pretreated with W@V-NPs (20 μg WOG/mL for 24 h) were further incubated with fresh medium for different

times. Then cells were collected to characterize Mfsd2a using Western blotting.

At the *in vivo* level, to evaluate whether W@V-NPs could affect Wnt signaling and Mfsd2a, 4T1Br model mice (intracranial injection method) were given intravenous injections of either WOG or W@V-NPs (5 mg/kg, daily, 7 times). At 24 h after the last injection, mice were intravenously injected with 100 µL of PE rat anti-mouse CD31 and brains were excised at 1 h after antibody injection. Then 20-µm-thick sections were stained for LEF1 or Mfsd2a and imaged under a confocal laser scanning microscope.

2.7. BTB penetration of O@V-NPs after pretreatment with W@V-NPs

BTB endothelial cells monolayer cultured in 6 well plates were first treated with either V-NPs or W@V-NPs (20 µg WOG/mL) for 24 h and then incubated with doxorubicin-labeled NPs and V-NPs (5 µg doxorubicin/mL) for 3 h. The cellular uptake was measured using flow cytometry. To investigate whether W@V-NPs could assist V-NPs in penetrating the BTB and entering 4T1Br brain metastatic tumor cells, at 48 h after 4T1Br plating in the BTB Transwell model (the establishment methods shown in Section 2.5), the medium was changed to 4T1Br TCM for 24 h. Then either V-NPs or W@V-NPs were added into the upper chamber for a further 24 h culture. Then IR780 and doxorubicin coloaded NPs and V-NPs in the control medium or 4T1Br TCM were added into the upper chamber (4 µg IR780 and 5 µg doxorubicin/mL). After 6 h incubation, IR780 and doxorubicin were measured for their distribution.

To evaluate the *in vivo* efficiency of targeting brain metastases, after the onset of neurological symptoms, 4T1Br model mice (intracranial injection method) were intravenously injected with first W@V-NPs (5 mg WOG/kg) and then O@V-NPs (5 mg WOG/kg) with intervals of 0, 6, 12, 24, 48, 72, and 96 h. At 2 after injections of O@V-NPs, blood serum, healthy brains, and metastatic tumors were harvested and analyzed for ORL content using LC−MS. For audiovisual and qualitative evaluation, 231Br model mice (intracardiac injection method) were given intravenous injections of first W@V-NPs (daily 5 mg WOG/kg for 7 days) and then doxorubicin-loaded NPs or V-NPs (10 mg doxorubicin/kg). At 12 h after injection of doxorubicin NPs, mice were perfused and excised brains were further fixed, dehydrated, and then sliced into 20-µm-thick sections for imaging under a confocal laser scanning microscope.

2.8. Therapeutic benefits of WO@V-NPs in mice with breast cancer brain metastases

Intracardiac injection allows widespread tumor cell distribution throughout the body of the animals and may produce metastases in sites other than the cerebral target compared with local implantation[26,27,35]. However, direct intracranial injection only allows metastatic tumor growth inside the brain and has higher reproducibility[21,35]. The local inoculation model is also a widely used model for brain metastases[21,36-38] and thus was used here for studying the therapeutic benefits. Three days after intracranial injection of luciferase-expressing 4T1Br cells, mice were intravenously treated with saline, V-NPs, W@V-NPs, ORL, O@V-NPs, and WO@V-NPs at a dose of 5 mg WOG and 5 mg ORL/kg every 3 days. Mice were continuously treated and monitored for survival and body weight until one of the following criteria for euthanasia was met: 1) the body weight of the mouse

dropped by 15% of its initial weight, or 2) the mouse became lethargic or sick and unable to feed. To investigate the survival benefits, three mice of each group were imaged for luciferase to indicate brain metastases. To study the *in vivo* therapeutic mechanisms, randomly selected mice in therapeutic experiments were sacrificed on Day 16 to obtain 20-µm-thick cerebral sections for whole-brain fluorescence imaging and apoptosis marker cleaved caspase 3 staining (CC3, TUNEL staining assay kit), and to collect the intracranial metastatic tumors for FAS activity measurement using an assay kit (BC0550, Solarbio life sciences) and LEF1 characterization using Western blotting.

2.9. Safety evaluation of WO@V-NPs

To investigate the *in vivo* safety of WO@V-NPs, ICR mice were administered intravenous W@V-NPs (15 mg WOG/kg, every 2 days from Days 2−14), intravenous WO@V-NPs (15 mg WOG and 10 mg ORL/kg, every 2 days from Days 2−14), or oral LGK974 (28.8 mg/kg, daily from Days 1−14). For behavioral studies, all mice were trained by being exposed to two identical cubes for 10 min on Day 12 for novel object recognition (NOR) and on Day 13 for object location test (OLT). At 1.5 h after training on Day 12, mice were evaluated for NOR by being exposed to one familiar object and one new object for 10 min to register the exploration time for each object. On Day 14 (at 24 h after training on Day 13), mice were evaluated for OLT by being exposed to two familiar objects with one in the initial location and the other in a new location for 5 min. During behavioral studies, distances between objects and walls were kept unchanged to avoid thigmotaxis influence. The exploration area was defined as the 40 cm × 40 cm area centered on the object. The preference percentages were calculated as the ratio of exploration time for the new object (or new position of the object) to the sum of exploration time for both objects. After behavioral studies, blood samples were collected 24 h after the last injection for routine blood tests and liver and kidney function evaluation. Major organs were then excised for hematoxylin−eosin staining and albumin staining for analyses of peripheral organ toxicity and brain edema (albumin leakage).

2.10. Statistical analysis

All quantitative data are presented as the mean ± standard deviation (SD). One-tailed unpaired Student's *t*-test or log-rank (Mantel−Cox) test was performed to determine statistical significance. The log-rank (Mantel−Cox) test was used to compare treatment groups in the survival study. Unpaired Student's *t*-test was used for other studies. All statistical tests were performed in GraphPad Software (Prism 8.0.1). ns indicates not significant, and $P < 0.05$ (*), 0.01 (**), and 0.001 (***) are considered significant.

3. Results

3.1. ORL efficiently induces apoptosis of breast cancer cells cultured in the lipid-depleted medium by inhibiting FAS

FAS expression and activity in brain metastatic breast cancers were shown to be significantly higher than that in healthy brains and primary breast cancers (Fig. 1A−C). To imitate the differentiated FAS activity at the *in vitro* level, breast cancer cells were cultured in different mediums. Compared with those in the control
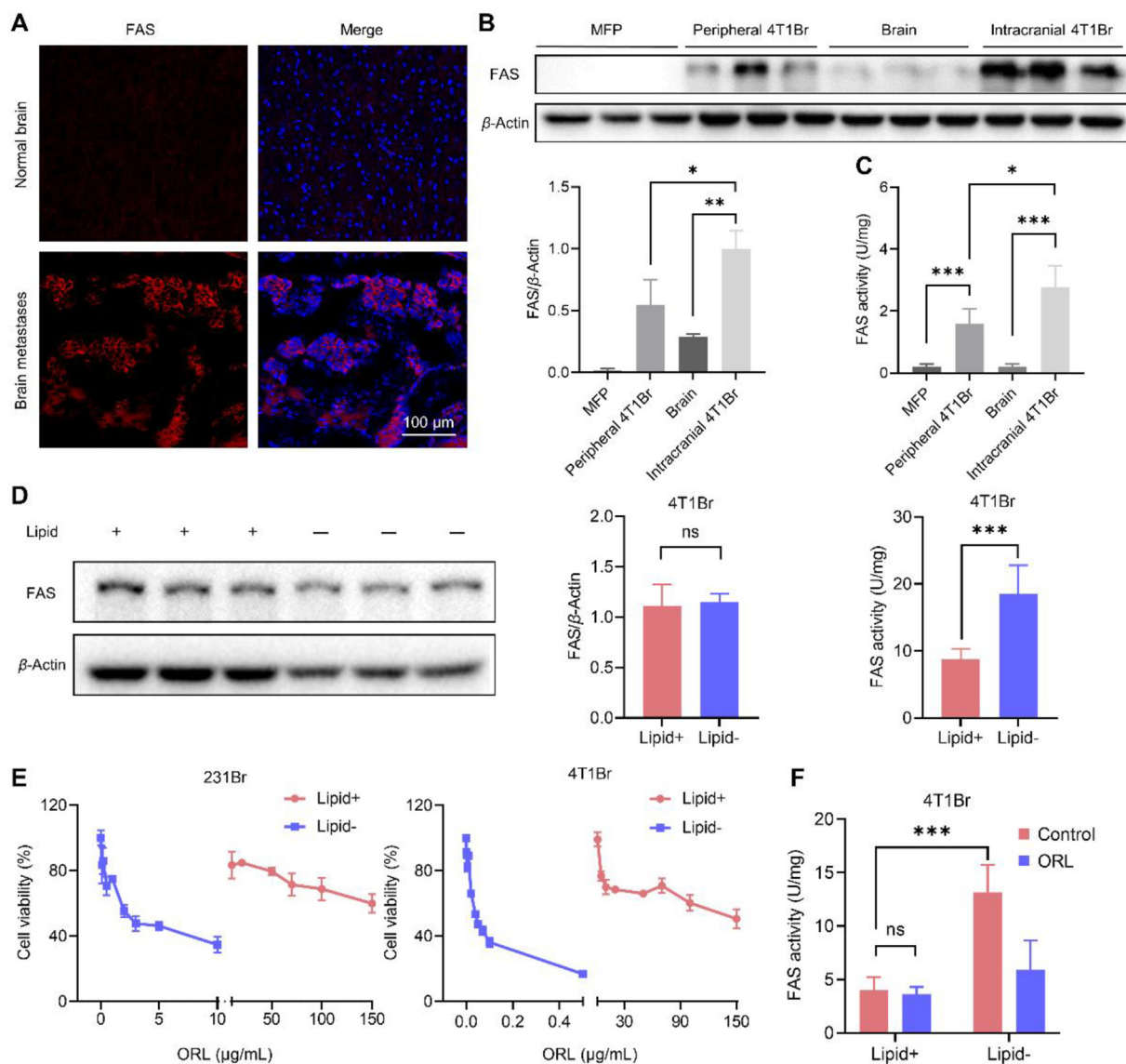
Figure 1 FAS expression and activity and therapeutic sensitivity of brain-metastatic breast cancer. (A) Intracranial FAS expression in model mice with 231Br brain metastases (intracardiac injection). Scale bar = 100 μm. Intracranial and mammary FAS expression (B) and activity (C) in model mice with 4T1Br brain metastases (intracranial injection). MFP stands for the mammary fat pad. Data are presented as mean ± SD ($n = 3$ in B, $n = 4$ in C). (D) FAS expression and activity of 4T1Br cells in different mediums. Data are presented as mean ± SD ($n = 5$). (E) Cytotoxicity of ORL on 231Br cells and 4T1Br cells in different environments. Data are presented as mean ± SD ($n = 5$). (F) Effects of ORL on FAS activity in 4T1Br cells in different mediums. Quantitative analysis was performed using ImageJ. Data are presented as mean ± SD ($n = 5$). *$P < 0.05$. **$P < 0.01$. ***$P < 0.001$. ns, not significant.

medium, breast cancer cells showed comparable FAS expression but enhanced activity in the brain-specific lipid-depleted micro-environment (Fig. 1D). Routine chemotherapeutic drugs (*e.g.*, doxorubicin and cisplatin) have been used in treating breast cancer brain metastases [28,39,40]. Both drugs were found less effective in killing cancer cells in−lipid medium (IC$_{50}$ on 231Br cells, 498 ng/mL and 17.1 μg/mL) than in +lipid medium (162 ng/mL and 5.0 μg/mL, Supporting Information Fig. S1). By contrary, ORL could bind with FAS and inhibit its enzymatic activity. ORL was found more effective in killing cancer cells in−lipid medium than in +lipid medium with IC$_{50}$ value of 48 ng/mL *versus* 150 μg/mL on 4T1Br cells (Fig. 1E and Supporting Information Fig. S2). ORL reduced FAS activity only in−lipid medium but not in +lipid medium (Fig. 1F). Collectively, these data proved

that ORL could efficiently kill breast cancer cells in lipid-deprived brain environment by inhibiting FAS activity and then can be used for treating brain metastases.

3.2. Characterization of W@V-NPs and O@V-NPs

O@V-NPs were designed to deliver ORL to brain metastases while W@V-NPs were developed to boost the BTB penetration ability of O@V-NPs. Based on the ultrasonic emulsification techniques [29,30,32,33,41], under the transmission electron microscope, both W@V-NPs and O@V-NPs exhibited regular spherical morphology (Fig. 2A). The hydrodynamic diameters of O@V-NPs and W@V-NPs reflected Gaussian distribution with their mean values of 115.6 nm and 112.9 nm (Fig. 2B−D). VCAM-1-
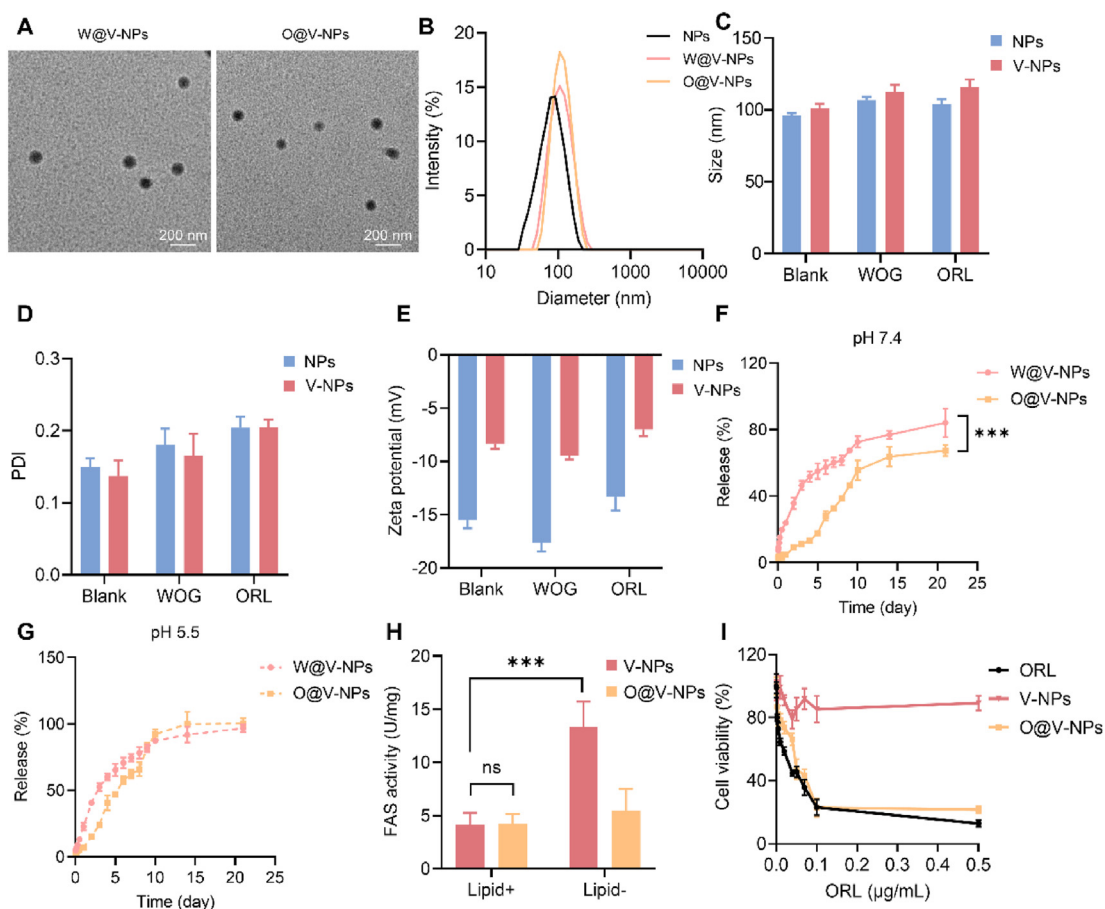
Figure 2 Physicochemical characterization of W@V-NPs and O@V-NPs. (A–E) Representative transmission electron microscope images, hydrodynamic diameters (distribution, mean, and polydispersity index) and Zeta potential of different NPs. Scale bar = 200 nm. Data are presented as mean ± SD ($n = 3$). (F, G) *In vitro* release of WOG and ORL from NPs in different pH. Data are presented as mean ± SD ($n = 3$). (H) Effects of O@V-NPs on FAS activity in 4T1Br cells in different mediums. Data are presented as mean ± SD ($n = 5$). (I) Cytotoxicity of O@V-NPs on 4T1Br cells in different environments. Data are presented as mean ± SD ($n = 5$). ***$P < 0.001$. ns, not significant.

targeting peptide ligand decreased Zeta potential (Fig. 2E), which may be related to its isoelectric point (pH 10.69) and is consistent with previous reports[42,43]. WOG and ORL were encapsulated with their respective loadings of 9.87% and 14.97% and released in a weak pH-sensitive manner (Fig. 2F and G). The release of WOG (48 h, 35.8% at pH 7.4 and 40.7% at pH 5.5) was faster than that of ORL (48 h, 9.3% at pH 7.4 and 15.6% at pH 5.5), which could be ascribed to relatively low hydrophobicity of WOG (log$P$ in octanol/water, 3.78 *versus* 4.40). Compared with V-NPs, O@V-NPs reduced FAS activity in the−lipid medium but not in the +lipid medium (Fig. 2H). O@V-NPs exhibited comparable tumor-inhibiting ability to ORL in a delipidated medium (Fig. 2I).

3.3. VCAM-1 mediates targeting of BTB and brain metastases

In model mice, VCAM-1 was shown around blood vessels and on tumor cells in brain metastases but not in healthy brains (Fig. 3A). At the *in vitro* level, VCAM-1 was especially expressed in BTB endothelial cells rather than BBB endothelial cells (Fig. 3B and C and Supporting Information Fig. S3A). At the *in vitro* level for 231Br brain metastases, VCAM-1 was highly expressed in 231Br BTB endothelial cells but not in 231Br cells (Fig. 3D). But for 4T1Br brain metastases, VCAM-1 was highly expressed in both 4T1Br BTB endothelial cells and 4T1Br cells (Fig. 3E and

Fig. S3B), suggesting the feasibility of utilizing VCAM-1 for targeting both 4T1Br BTB endothelial cells and metastatic 4T1Br cells. Compared with unmodified NPs, V-NPs were internalized more efficiently in BTB endothelial cells and 4T1Br cells rather than in BBB endothelial cells and 231Br cells (Fig. 3F and Supporting Information Fig. S4). V-NPs selectively penetrated the BTB and entered 4T1Br brain metastatic tumor cells (Fig. 3G and H and Supporting Information Fig. S5).

For pharmacokinetics studies, all formulations showed similar blood dynamical behaviors both in normal mice (Supporting Information Fig. S6A and Table S1) and in model mice (Fig. 3I). Notably, the blood IR780 fluorescence intensity−time curve for IR780@V-NPs (Fig. 3I, measured by the semi-quantitative *in vivo* imaging method) was shown consistent with the blood WOG concentration−time profile for W@V-NPs (Fig. 3J, measured by the quantitative LC−MS technique). For biodistribution studies in normal mice, in contrast to A-NPs, both unmodified NPs and V-NPs hardly penetrated healthy brains with their major distribution in livers and kidneys (Fig. S6B−S6D). In 4T1Br model mice, both IR780-loaded unmodified NPs and V-NPs were primarily distributed in livers and kidneys (Fig. 3K and L), which is in line with their distribution patterns in normal mice (Figs. S6C and S6D). However, compared with unmodified NPs, V-NPs more efficiently entered diseased brains with 4T1Br
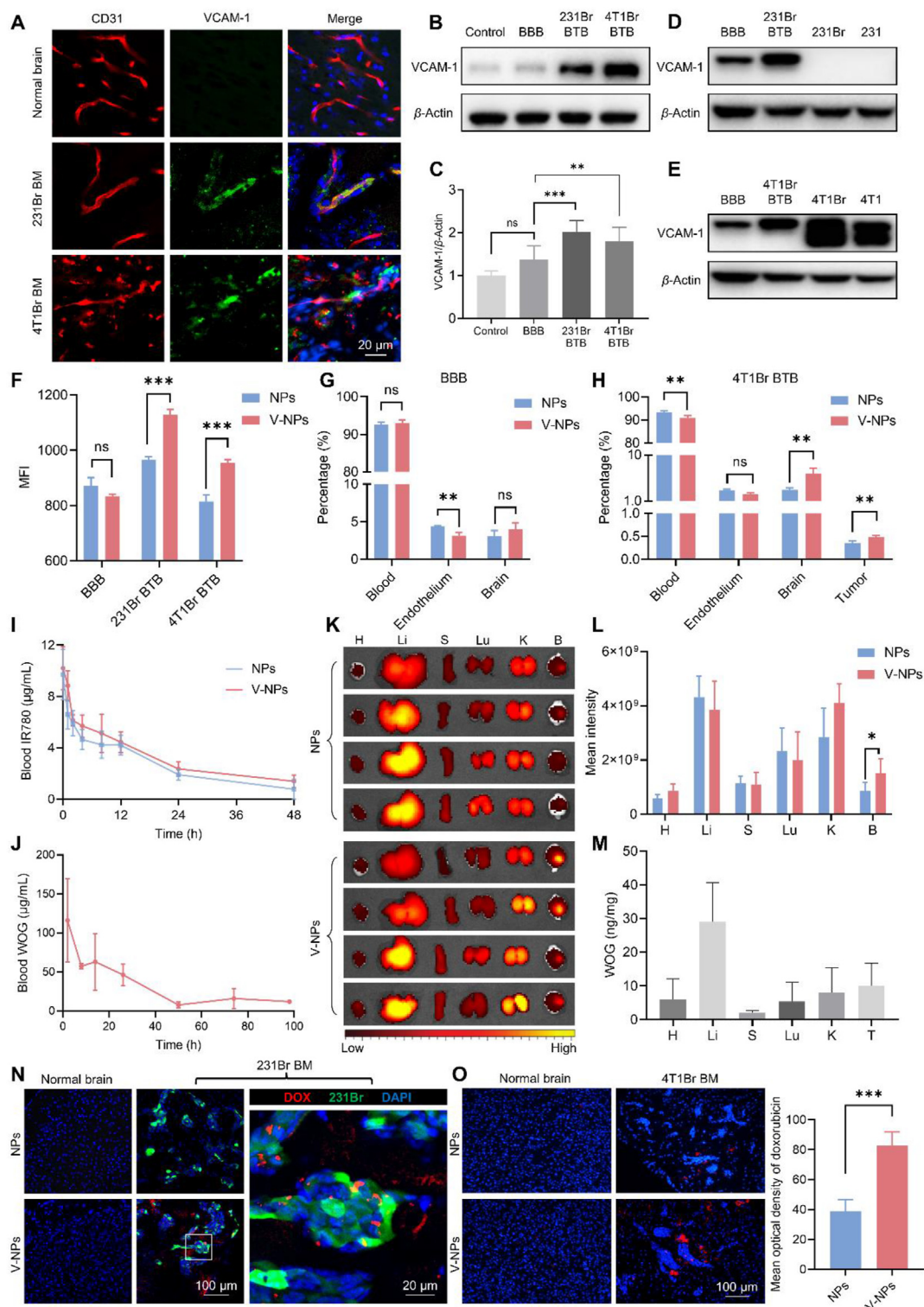
Figure 3 V-NPs could target BTB and brain metastases by binding with VCAM-1. (A) Intracranial VCAM-1 expression in model mice with brain metastases. Scale bar = 20 μm. (B–E) The expression of VCAM-1 in different cells. The bEND.3 cells were used as control. BBB endothelial cells were produced by incubating bEND.3 cells with conditioned medium from bEND.3 cells. BTB endothelial cells were produced by incubating bEND.3 cells with TCM. Quantitative analysis was performed using ImageJ. Data are presented as mean ± SD ($n = 5$). (F–H) *In vitro* cellular uptake and penetration across the BBB/BTB model. Data are presented as mean ± SD ($n = 3$ in F, G. $n = 4$ in H). (I–M) Pharmacokinetics and biodistribution of IR780-loaded formulations (I, K, and L, measured by the semi-quantitative *in vivo* imaging method) and W@V-NPs (J and M, measured by the quantitative LC−MS technique) in 4T1Br model mice. H, Li, S, Lu, K, B, and T represent heart, liver, spleen, lung, kidney, brain, and intracranial metastatic tumor, respectively. Data are presented as mean ± SD ($n = 6$). (N, O) Intracranial distribution of various NPs in model mice with breast cancer brain metastases. Scale bar = 100 or 20 μm (enlarged area). Data are presented as mean ± SD ($n = 6$). **$P < 0.01$. ***$P < 0.001$. ns, not significant.

brain metastases (Fig. 3K and L), suggesting their preferential distribution in intracranial metastatic tumors. Moreover, the distribution pattern of WOG@V-NPs was found comparable to that of IR780-loaded V-NPs (Fig. 3L and M), and WOG was detected in intracranial metastatic tumors but not in normal brains (Fig. 3M). More deeply from a microscopic perspective, V-NPs efficiently and especially penetrated brain metastases rather than in healthy brains (Fig. 3N and O). These data suggest that, through targeting VCAM-1, V-NPs could mediate selective BTB penetration to deliver drugs to both BTB and brain metastases.

3.4. W@V-NPs regulate BTB Wnt signaling and subsequent expression of transcytosis-controlling Mfsd2a

Wnt signaling controls Mfsd2a expression in the BBB/BTB and its activation upregulates Mfsd2a and suppresses BBB/BTB

transcytosis. LEF1 is a marker of Wnt activation. Through LEF1 staining, Wnt signaling was found activated in BTB endothelial cells and relatively silent in BBB endothelial cells (Fig. 4A). While the expression of Mfsd2a was found to be regulated by Wnt signaling (Supporting Information Fig. S7), comparable levels of Mfsd2a were found between Wnt agonist LiCl-treated cells and BTB endothelial cells (Fig. 4B). Small molecule Wnt inhibitor WOG was shown to silence Wnt signaling and downregulate Mfsd2a in both types of BTB endothelial cells and LiCl-treated cells in a concentration-dependent manner or the form of W@V-NPs (Fig. 4C and D and Supporting Information Fig. S8). We determined the half-life of Mfsd2a in bEND.3 cells by using a translation-blocking reagent cycloheximide and quantifying Mfsd2a levels. Intrinsic turnover half-life of Mfsd2a in bEND.3 cells was found to be ∼2.7 h, while cells treated with W@V-NPs showed degradation half-life of ∼12.3 h
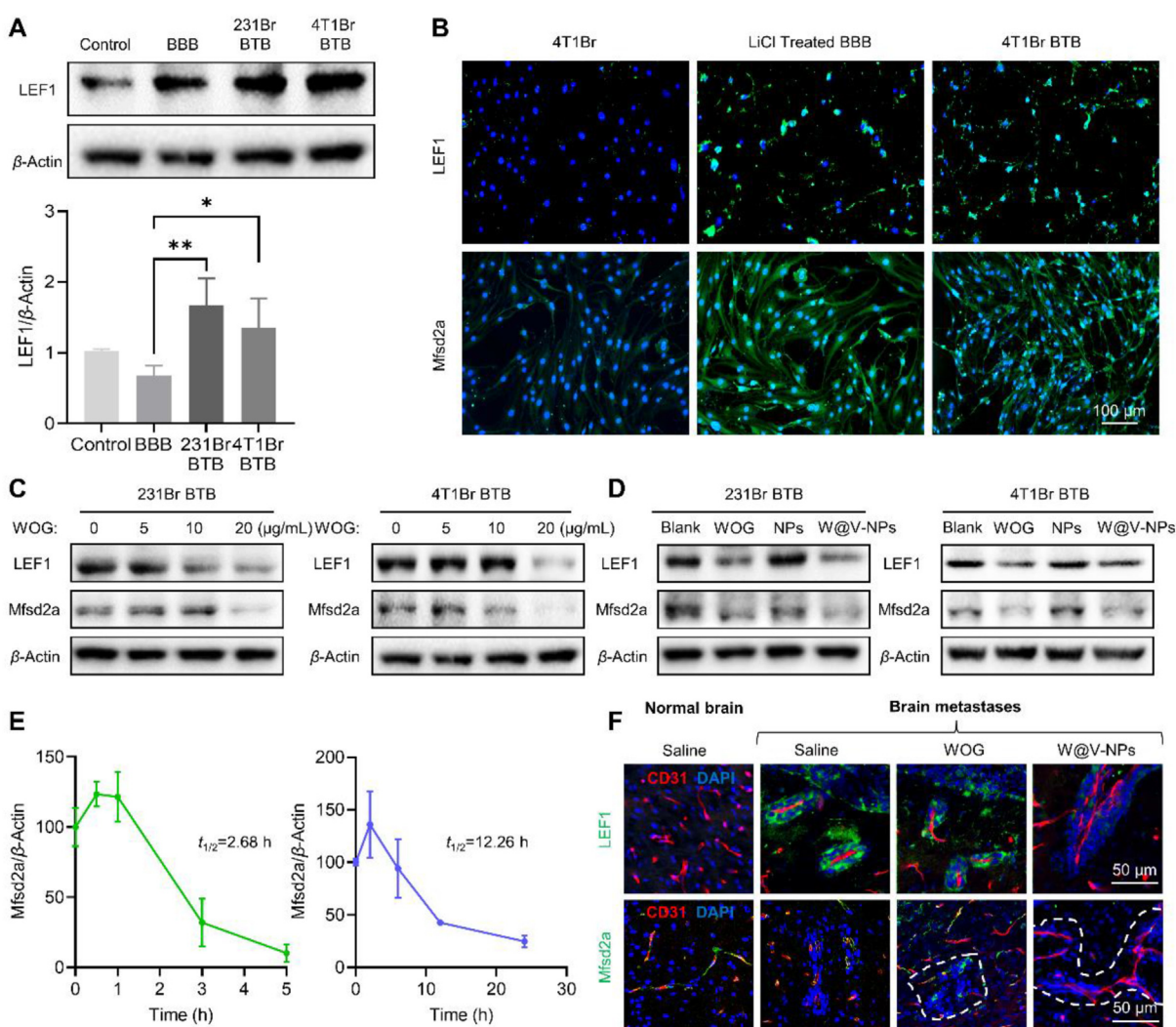

Figure 4 W@V-NPs regulate BTB Wnt signaling and Mfsd2a expression. (A, B) The status of Wnt signaling in BBB/BTB endothelial cells and tumor cells was evaluated by staining LEF1. The bEND.3 cells were used as control. Scale bar = 100 μm. Data are presented as mean ± SD ($n = 4$). (C, D) Effects of WOG and W@V-NPs on Wnt signaling and Mfsd2a expression in BTB endothelial cells were evaluated. (E) Time dependency of Mfsd2a regulation by W@V-NP-regulated in bEND.3 cells. Cells treated with the translation-blocking reagent cycloheximide were used as control. Data are presented as mean ± SD ($n = 3$). (F) Effects of WOG and W@V-NPs on intracranial Wnt signaling and Mfsd2a expression in model mice with 4T1Br brain metastases were evaluated. Scale bar = 50 μm *$P < 0.05$. **$P < 0.01$.

(Fig. 4E and Supporting Information Fig. S9). Mfsd2a recovered to initial levels at ~36 h after washout of W@V-NPs (Supporting Information Fig. S10).

We further studied whether W@V-NPs could regulate the Wnt signaling and Mfsd2a at the *in vivo* level. Wnt signaling was found relatively silent in healthy brain regions but activated in brain metastases in model mice (Fig. 4F). Both WOG and W@V-NPs did not change the status of Wnt signaling in healthy brain regions. However, W@V-NPs silenced the activated Wnt signaling in brain metastases. In contrast to Wnt signaling, Mfsd2a was expressed comparably in healthy brain regions and brain metastases. There was no change of Mfsd2a expression in healthy brain regions after treatments with either WOG or W@V-NPs. However, the expression of Mfsd2a in brain metastases was reduced by W@V-NPs but not by WOG. Collectively, W@V-NPs could selectively regulate the Wnt signaling and Mfsd2a around brain metastases.

3.5. W@V-NPs for boosting BTB penetration of following O@V-NPs

Inspired by the special regulation of BTB Wnt signaling and Mfsd2a levels, we next investigated if W@V-NPs could boost

BTB penetration of O@V-NPs for improved drug delivery. The uptake of V-NPs in BTB endothelial cells was found to be increased by preincubation with W@V-NPs (Fig. 5A). BTB penetration and brain metastatic tumor cell uptake of V-NPs were also improved by the same preprocessing (Fig. 5B and Supporting Information Fig. S11), suggesting the release of Mfsd2a-inhibited BTB endocytosis and transcytosis. Through measuring ORL concentration, we found the concentration ratio of ORL in brain metastases to ORL in blood was higher than the concentration ratio of ORL in healthy brain regions to ORL in blood (Fig. 5C). We also confirmed pretreatment with W@V-NPs enhanced the concentration of V-NPs in brain metastases rather than in healthy brain regions (Fig. 5D−F).

3.6. Therapeutic benefits

Inspired by the discovery that W@V-NPs could specially regulate BTB Wnt signaling and Mfsd2a and then boost NPs' BTB penetration, we next studied if W@V-NPs could enhance the therapeutic benefits of O@V-NPs. Model mice were treated to explore the therapeutic benefits of WO@V-NPs by monitoring animal survival and the progression of 4T1Br brain metastases (imaging luciferase and the isolated whole brain). Compared with saline and V-NPs (no
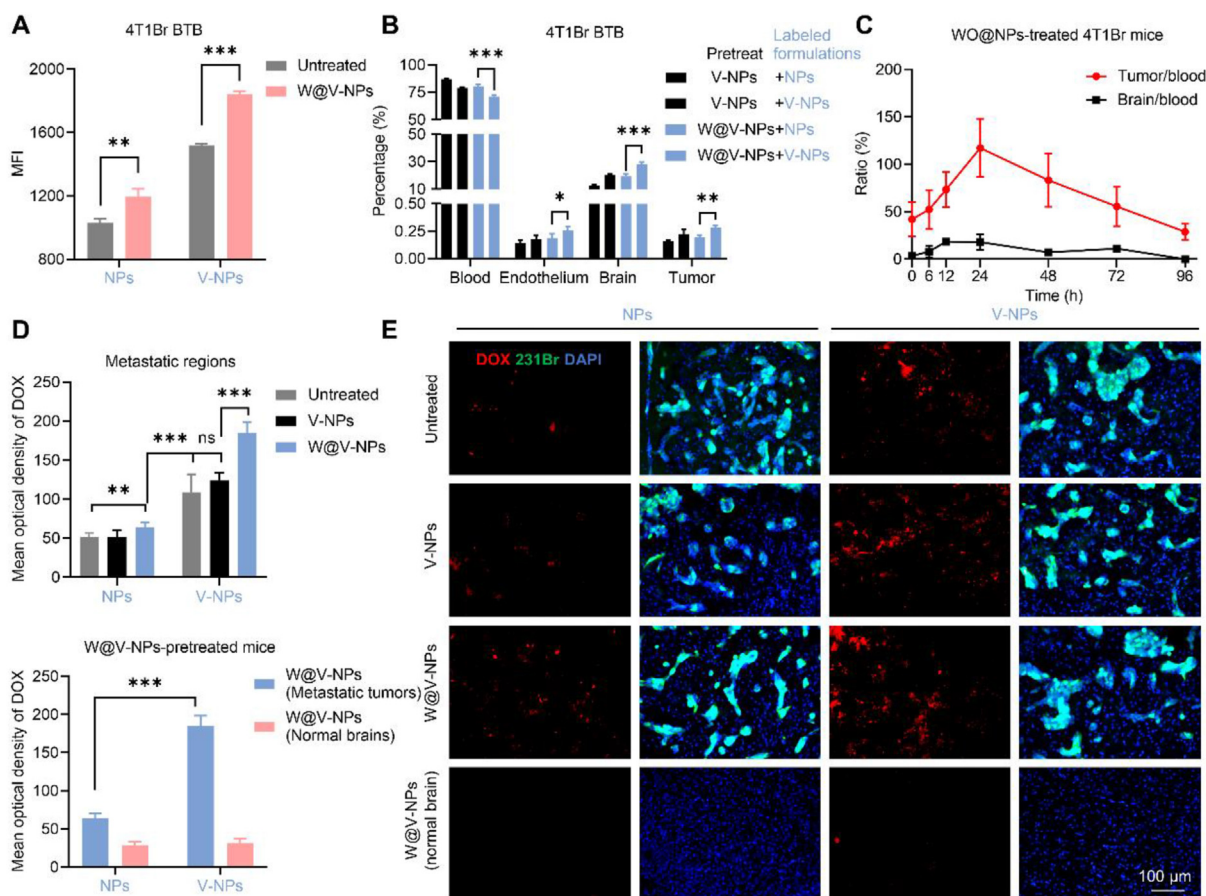

Figure 5 Effects of W@V-NPs on endocytosis and transcytosis in BTB endothelial cells. (A, B) *In vitro* cellular uptake and penetration of V-NPs in 4T1Br BTB endothelial cells after treatments with W@V-NPs. Data are presented as mean ± SD ($n = 3$ in A, $n = 4$ in B). (C) Distribution ratios of O@V-NPs across different regions in 4T1Br model mice, which were pretreated with W@V-NPs. Data are presented as mean ± SD ($n = 4$). (D, E) The accumulation of NPs and V-NPs in metastatic regions and normal brain regions in 231Br model mice after pretreatments with different formulations. Scale bar = 100 μm. Data are presented as mean ± SD ($n = 6$). *$P < 0.05$. **$P < 0.01$. ***$P < 0.001$. ns, not significant.
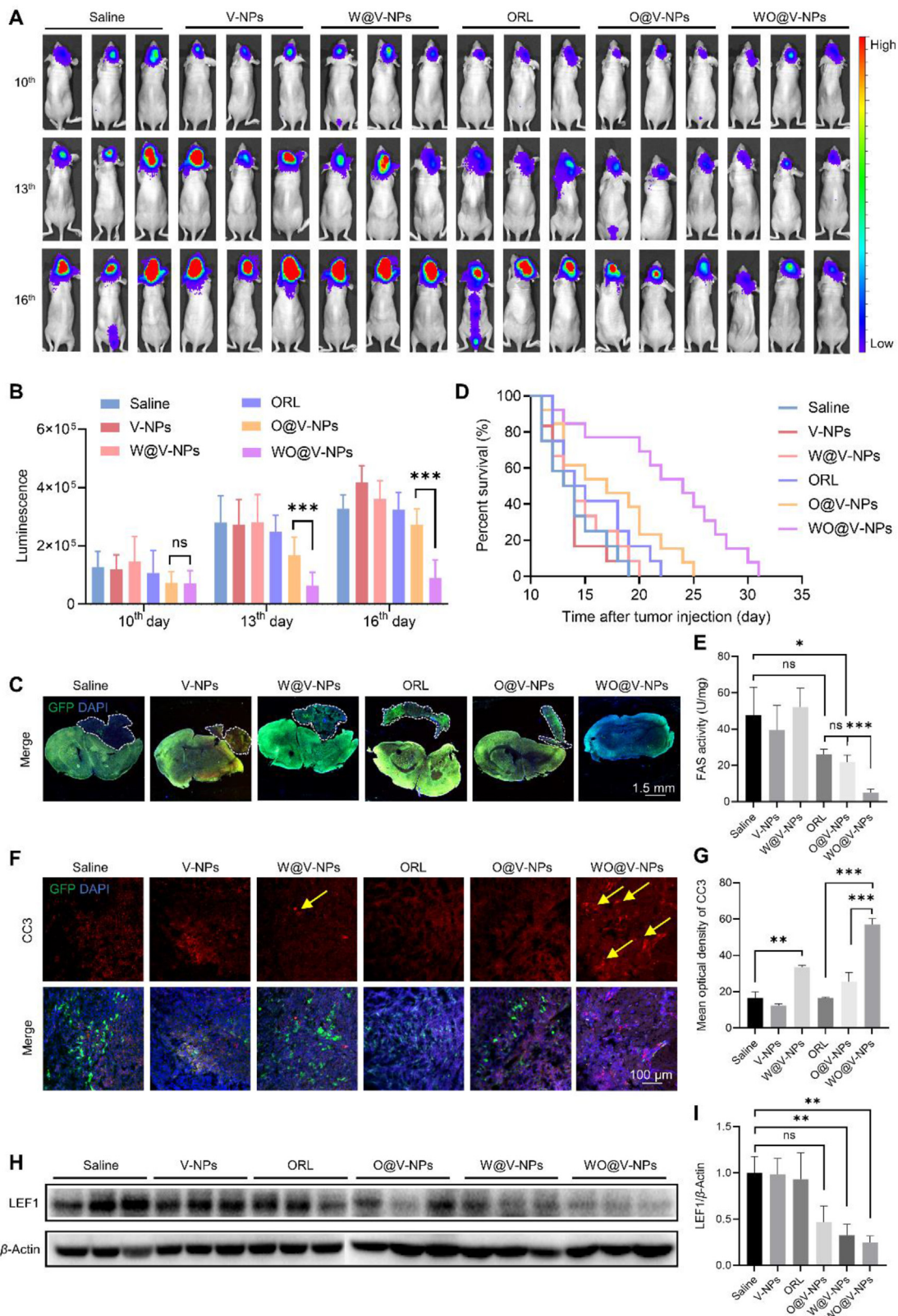
Figure 6 Therapeutic benefits of WO@V-NPs in model mice with 4T1Br brain metastases. (A, B) Representative images of the development of 4T1Br brain metastases imaged by IVIS. The bioluminescence intensity was quantified using Living Image 3.0. Data are presented as mean $\pm$ SD ($n = 9$). (C) Representative fluorescence images of whole-brain sections isolated from mice sacrificed on Day 16 in therapeutic experiments. Scale bar = 1.5 mm. (D) Kaplan−Meier survival curves of model mice received the indicated treatments. (E) FAS activity in intracranial metastatic tumors excised from mice sacrificed on Day 16 in therapeutic experiments. Data are presented as mean $\pm$ SD ($n = 5$). (F, G) CC3 staining (apoptosis) of brain sections collected from mice sacrificed on Day 16 in therapeutic experiments. Scale bar = 100 μm. Data are presented as mean $\pm$ SD ($n = 3$). (H, I) LEF1 staining (the status of Wnt signaling) of brain sections obtained from mice sacrificed on Day 16 in therapeutic experiments. Data are presented as mean $\pm$ SD ($n = 3$). *$P < 0.05$. **$P < 0.01$. ***$P < 0.001$. ns, not significant.

benefit), both ORL and O@V-NPs did not show any therapeutic effect (Fig. 6A−C), indicating the absence of the enhanced permeability and retention effect in breast cancer brain metastases and the low transport efficiency of just targeting VCAM-1. Day 13, while Wnt-inhibiting W@V-NPs did not produce any effect (100.7%), WO@V-NPs improved the quality of life of mice and markedly restricted intracranial tumor growth with tumor signal 25.2% and 36.4% of ORL and O@V-NPs treated mice. On Day 16, the relative growth became 27.9% and 33.4% of ORL and O@V-NPs treated mice. Whole-brain fluorescence imaging data confirmed that treatments with WO@V-NPs delayed the growth of intracranial metastatic tumors with the highest efficiency (Fig. 6C). With the obvious growth-inhibiting effect, the median survival time for mice treated with WO@V-NPs was extended to 24 days, which is evidently longer than that for mice treated with saline (13.5 days), V-NPs (13.5 days), W@V-NPs (13.5 days), ORL (14.5 days), and O@V-NPs (17 days) (Fig. 6D).

To explain the *in vivo* therapeutic mechanisms, FAS activity, cell apoptosis, and the status of Wnt signaling were evaluated for intracranial metastatic tumors collected from mice given various treatments. Although O@V-NPs markedly reduced FAS activity in brain metastases compared with saline, there was no statistical difference in FAS activity between free ORL and O@V-NPs (Fig. 6E). Notably, WO@V-NPs dramatically diminished the FAS activity in brain metastases with the efficiency significantly higher than that of O@V-NPs, heralding the improved lipogenesis inhibition. According to the data of CC3 staining, mice treated with WO@V-NPs showed more tumor cell apoptosis than those given free ORL or O@V-NPs (Fig. 6F and G), implying lipogenesis inhibition and lipid deprivation mediated cell apoptosis, which is consistent with the *in vitro* therapeutic data (Fig. 1E and Supporting Information Fig. S2). W@V-NPs were also shown to induce tumor apoptosis (Fig. 6F and G), which could be ascribed to the inactivation of tumor Wnt signaling (Fig. 6H and I).

Mice treated with WO@V-NPs showed the latest loss of body weight (Fig. S12), also suggesting the intervention of progress of breast cancer brain metastases. Notably, intravenous injection of the weight-loss drug ORL did not induce mouse weight loss during therapeutic experiments (Fig. S12), which can be ascribed to the validity of its full pharmacologic effects only in the gastrointestinal tract. It has been reported that ORL reduces body weight by forming a covalent bond with the active serine site of gastric and pancreatic lipases in the lumen of the gastrointestinal tract to directly inhibit these enzymes to decrease the absorption of dietary fat[44]. This covalent inhibition of these enzymes prevents the hydrolysis of dietary fat into absorbable free fatty acids and monoglycerols[44].

3.7. Safety evaluation of WO@V-NPs

It has been reported that, after the knockout of astrocytic Wnt, mice were shown to develop brain edema[45], which is characterized by extravasation of serum proteins into the brain[46]. Although the modulation of Wnt signaling and Mfsd2a is orientated to the BTB, it is necessary to check whether W@V-NPs would induce edema in healthy brains, which is associated with BBB opening. After multiple intravenous injections of W@V-NPs in healthy mice, no leakage of serum albumin (∼68 kD) was found in the brain cortex and hippocampus (Fig. 7A), confirming the BTB-targeting effect of W@V-NPs. Behavioral studies including NOR and OLT were performed to examine whether WO@V-NPs would induce

cognitive impairments, *e.g.*, learning and recognition memory (Fig. 7B). Oral Wnt inhibitor LGK974 was used as a control[47]. In the NOR training phase, all mice explored both objects equally with no difference in the object preference index. In the NOR testing phase, all mice explored new objects equally. In both the training phase and testing phase of OLT, all mice comparably explored objects at new positions, indicating that no cognitive deficit and memory defect was induced by all treatments. Collectively, multiple injections of WO@V-NPs did not impair short-term object memory and long-term location memory.

Wnt signaling is also crucial for cellular stemness, which plays an important role in maintaining normal physiological functions of bone marrow, intestine, stomach, and skin[47]. To examine the effects of WO@V-NPs on normal homeostasis of Wnt-dependent tissues, a set of mouse toxicology studies was performed in healthy mice. According to the whole blood cell counts, all groups of mice showed blood cell levels within the normal ranges (Supporting Information Fig. S13), indicating that no systemic anemia or inflammation occurred and no effect of inhibiting Wnt signaling on hemopoietic stem cells in the bone marrow. According to the data of hematoxylin-eosin staining, LGK974 (20 mg/kg per day for 14 days) caused loss of gastric epithelial cells in the stomach, loss of intestinal epithelium and shortening of villi in duodenum and ileum, and changes in the hair follicle, spleen, and hepatic sinusoid (Fig. 7D and Supporting Information Fig. S14), which is consistent with previous report[47]. However, although some liver dysfunctions were shown from the serum biochemical parameter analyses (Fig. 7E), which can be ascribed to the liver accumulation of V-NPs (Figs. S6C and S6D, and Fig. 3K−M), both W@V-NPs and WO@V-NPs were well-tolerated without abnormal histopathological findings in Wnt-dependent tissues including intestine, stomach, skin, and liver. While LGK974 induced body weight loss, all other mice showed similar patterns of body weight (Fig. 7C), indicating low peripheral toxicity. Collectively, these data confirmed the biocompatibility for intravenous administration of W@V-NPs for BTB modulation and WO@V-NPs for treatment against brain metastases.

4. Discussion

The brain has low environmental lipids relative to peripheral tissues, which propels primary or metastatic brain tumors to express lipogenesis proteins to synthesize lipids for intracranial tumor growth[1,48]. This imposed lipogenesis dependency suggests the potential of metabolic therapy against brain metastases. Our finding confirmed the therapeutic advantage of lipase inhibitors over conventional chemotherapeutic drugs in inhibiting breast tumor growth in low-lipid environments. FAS is upregulated and necessary in many types of brain cancers including malignant meningioma, glioma, and other brain metastases[49-51], suggesting the therapeutic feasibility of applying the FAS inhibition strategy in these tumors. It should also be noted that tumor cells may form resistance to lipogenesis inhibition *via* salvaging fatty acids from existing brain lipids[1], which explains the delayed tumor growth in therapeutic experiments.

The BTB activates its Wnt signaling to maintain Mfsd2a expression and control transcellular vesicular transport[11,45,52-56]. We found Wnt signaling was relatively silent in the BBB and healthy brains but activated in the BTB and brain metastases. Considering the specific expression of VCAM-1 in the BTB and brain metastases, we proposed the design of VCAM-1-targeting
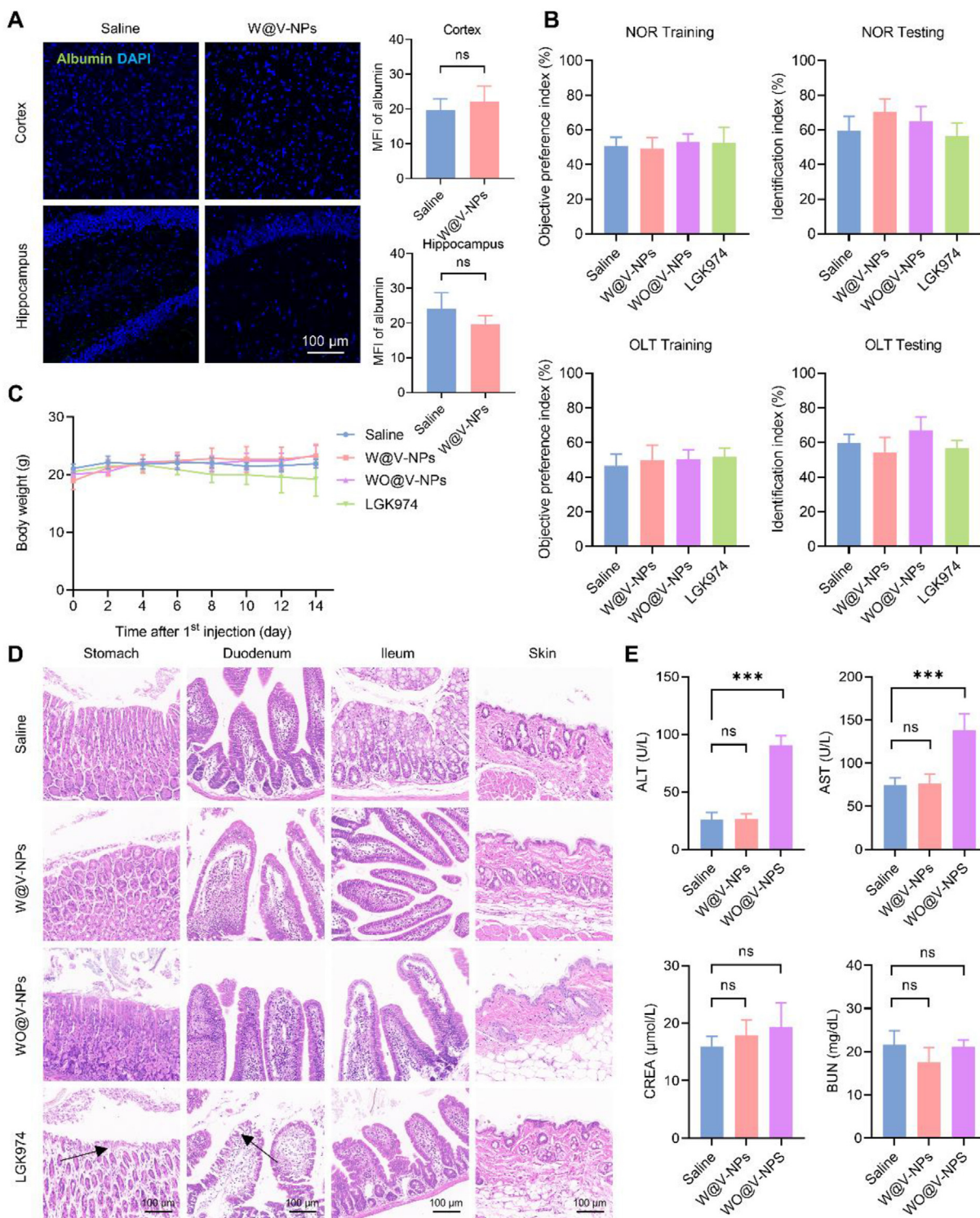
Figure 7 Safety evaluation of WO@V-NPs. (A) Effects of W@V-NPs on normal BBB permeability were evaluated by staining blood component albumin, which normally cannot enter brain parenchyma. Scale bar = 100 μm. Data are presented as mean ± SD ($n = 5$). (B) Effects of W@V-NPs on learning and recognition memory of normal mice were evaluated by investigating the ratio of exploration time for the new object (or new position) to the sum of exploration time. Data are presented as mean ± SD ($n = 10$). (C) Body weights of mice after various treatments. Data are presented as mean ± SD ($n = 10$). (D) Hematoxylin-eosin staining was performed for various organs of normal mice, which were given different formulations, to evaluate the effects on tissue morphologies. Scale bar = 100 μm. (E) Blood markers of liver functions and kidney functions were quantitatively measured. Data are presented as mean ± SD ($n = 5$). ***$P < 0.001$. ns, not significant.

WO@V-NPs to boost BTB transcellular transport *via* suppressing BTB Wnt signaling and downregulating Mfsd2a, to intensify drug delivery and inhibit lipogenesis of brain metastases. Many brain-targeted NPs and nutrients permeate through the BBB *via* caveolae-mediated transcytosis[13,57]. Reducing the levels of BTB Mfsd2a through inactivating BTB Wnt could regulate endothelial cell lipid composition and promote caveolae-mediated transcytosis and then may increase BTB permeability to all these caveolae-involved transcellularly transported substances. Fortunately, the increased transport is restricted to the BTB, and blood-borne substances such as albumin were not found in normal brains (Fig. 7A), demonstrating specificity and safety. More importantly, most brain-targeted drug delivery strategies are directed against whole-brain microvessels rather than specific BTB to boost transcellular transport into the brain such as Mfsd2a inhibition and LRP1 upregulation[13,30,58,59]. In this study, W@V-NPs specifically accelerated transcellular transport across the BTB rather than the BBB *via* inactivating BTB-specific Wnt signaling.

Wnt signaling is also involved in the expression regulation of tight junction proteins and active efflux transporters besides Mfsd2a[56,60-65], suggesting that W@V-NPs may improve the transport of small molecules into brain metastases. It has been reported Wnt inhibitor factor 1 diminishes BTB Wnt signaling and improves medulloblastoma responses to small-molecule drugs[15,66-70]. BTB also expresses other permeability modulators including ATP-sensitive potassium channels, bradykinin B2 receptors, and adenosine receptors[29,71-75]. VCAM-1-based BTB-targeting strategy can be used to deliver related drugs to optimize BTB modulation.

5. Conclusions

WO@V-NPs were developed and demonstrated to be able to especially modulate BTB and efficiently deliver lipogenesis inhibition for effective therapy against breast cancer brain metastases. More importantly, WO@V-NPs did not induce brain edema, cognitive impairment, or systemic toxicity in healthy mice. Considering that brain metastases are not amenable to surgical resection and are often responsible for patient relapse and death, WO@V-NPs hold the potential for systemic treatments of brain metastases. The therapeutic strategy of combining BTB regulation with brain-specific therapy is also expected to provide new directions for other brain diseases.

Acknowledgments

Author contributions

Liang Han designed the research. Yang Tong, Pei An, Puxian Tang, Rui Mu, Yuteng Zeng, Hang Sun, Mei Zhao, Ziyan Lv and Pan Wang carried out the experiments and performed data analysis. Wanjun Han and Chunshan Gui participated part of the experiments. Liang Han and Xuechu Zhen wrote the manuscript and revised the manuscript. All of the authors have read and approved the final manuscript.

Conflicts of interest

The authors have no conflicts of interest to declare.

Appendix A.   Supporting information

Supporting data to this article can be found online at https://doi.org/10.1016/j.apsb.2024.03.024.

References

1. Ferraro GB, Ali A, Luengo A, Kodack DP, Deik A, Abbott KL, et al. Fatty acid synthesis is required for breast cancer brain metastasis. *Nat Can (Ott)* 2021;**2**:414−28.
2. Mills MN, Figura NB, Arrington JA, Yu HM, Etame AB, Vogelbaum MA, et al. Management of brain metastases in breast cancer: a review of current practices and emerging treatments. *Breast Cancer Res Treat* 2020;**180**:279−300.
3. Achrol AS, Rennert RC, Anders C, Soffietti R, Ahluwalia MS, Nayak L, et al. Brain metastases. *Nat Rev Dis Prim* 2019;**5**:5.
4. Boire A, Brastianos PK, Garzia L, Valiente M. Brain metastasis. *Nat Rev Cancer* 2020;**20**:4−11.
5. Kabraji S, Ni J, Lin NU, Xie S, Winer EP, Zhao JJ. Drug resistance in HER2-positive breast cancer brain metastases: Blame the barrier or the brain? *Clin Cancer Res* 2018;**24**:1795−804.
6. Ruan S, Zhou Y, Jiang X, Gao H. Rethinking CRITID procedure of brain targeting drug delivery: circulation, blood brain barrier recognition, intracellular transport, diseased cell targeting, internalization, and drug release. *Adv Sci* 2021;**8**:2004025.
7. Song Y, Hu C, Fu Y, Gao H. Modulating the blood−brain tumor barrier for improving drug delivery efficiency and efficacy. *View* 2022;**3**:20200129.
8. Ngo B, Kim E, Osorio-Vasquez V, Doll S, Bustraan S, Liang RJ, et al. Limited environmental serine and glycine confer brain metastasis sensitivity to PHGDH inhibition. *Cancer Discov* 2020;**10**:1352−73.
9. Kridel SJ, Axelrod F, Rozenkrantz N, Smith JW. Orlistat is a novel inhibitor of fatty acid synthase with antitumor activity. *Cancer Res* 2004;**64**:2070−5.
10. Martin M, Vermeiren S, Bostaille N, Eubelen M, Spitzer D, Vermeersch M, et al. Engineered Wnt ligands enable blood−brain-barrier repair in neurological disorders. *Science* 2022;**375**:eabm4459.
11. Wang Z, Liu CH, Huang S, Fu Z, Tomita Y, Britton WR, et al. Wnt signaling activates MFSD2A to suppress vascular endothelial transcytosis and maintain blood-retinal barrier. *Sci Adv* 2020;**6**:eaba7457.
12. Ben-Zvi A, Lacoste B, Kur E, Andreone BJ, Mayshar Y, Yan H, et al. Mfsd2a is critical for the formation and function of the blood−brainbarrier. *Nature* 2014;**509**:507−11.
13. Ju X, Miao T, Chen H, Ni J, Han L. Overcoming Mfsd2a-mediated low transcytosis to boost nanoparticle delivery to brain for chemotherapy of brain metastases. *Adv Healthcare Mater* 2021;**10**:e2001997.
14. Xie Y, He L, Zhang Y, Huang H, Yang F, Chao M, et al. Wnt signaling regulates MFSD2A-dependent drug delivery through endothelial transcytosis in glioma. *Neuro Oncol* 2023;**25**:1073−84.
15. Phoenix TN, Patmore DM, Boop S, Boulos N, Jacus MO, Patel YT, et al. Medulloblastoma genotype dictates blood brain barrier phenotype. *Cancer Cell* 2016;**29**:508−22.
16. Nguyen DX, Chiang AC, Zhang XH, Kim JY, Kris MG, Ladanyi M, et al. WNT/TCF signaling through LEF1 and HOXB9 mediates lung adenocarcinoma metastasis. *Cell* 2009;**138**:51−62.

17. Valiente M, Obenauf AC, Jin X, Chen Q, Zhang XH, Lee DJ, et al. Serpins promote cancer cell survival and vascular co-option in brain metastasis. *Cell* 2014;**156**:1002−16.

18. Chung H, Jung YM, Shin DH, Lee JY, Oh MY, Kim HJ, et al. Anti-cancer effects of wogonin in both estrogen receptor-positive and -negative human breast cancer cell lines *in vitro* and in nude mice xenografts. *Int J Cancer* 2008;**122**:816−22.

19. Soto MS, Serres S, Anthony DC, Sibson NR. Functional role of endothelial adhesion molecules in the early stages of brain metastasis. *Neuro Oncol* 2014;**16**:540−51.

20. Liu HJ, Wang M, Shi S, Hu X, Xu P. A Therapeutic sheep in metastatic wolf's clothing: trojan horse approach for cancer brain metastases treatment. *Nano-Micro Lett* 2022;**14**:114.

21. Masmudi-Martin M, Zhu L, Sanchez-Navarro M, Priego N, Casanova-Acebes M, Ruiz-Rodado V, et al. Brain metastasis models: what should we aim to achieve better treatments? *Adv Drug Deliv Rev* 2021;**169**:79−99.

22. Palmieri D, Bronder JL, Herring JM, Yoneda T, Weil RJ, Stark AM, et al. Her-2 overexpression increases the metastatic outgrowth of breast cancer cells in the brain. *Cancer Res* 2007;**67**:4190−8.

23. Yoneda T, Williams PJ, Hiraga T, Niewolna M, Nishimura R. A bone-seeking clone exhibits different biological properties from the MDA-MB-231 parental human breast cancer cells and a brain-seeking clone *in vivo* and *in vitro*. *J Bone Miner Res* 2001;**16**:1486−95.

24. Woditschka S, Evans L, Duchnowska R, Reed LT, Palmieri D, Qian Y, et al. DNA double-strand break repair genes and oxidative damage in brain metastasis of breast cancer. *J Natl Cancer Inst* 2014;**106**:dju145.

25. Fitzgerald DP, Subramanian P, Deshpande M, Graves C, Gordon I, Qian Y, et al. Opposing effects of pigment epithelium-derived factor on breast cancer cell *versus* neuronal survival: implication for brain metastasis and metastasis-induced brain damage. *Cancer Res* 2012;**72**:144−53.

26. Bussard KM, Mastro AM. *Ex-vivo* analysis of the bone microenvironment in bone metastatic breast cancer. *J Mammary Gland Biol Neoplasia* 2009;**14**:387−95.

27. Kang Y. Analysis of cancer stem cell metastasis in xenograft animal models. *Methods Mol Biol* 2009;**568**:7−19.

28. Ni J, Miao T, Su M, Khan NU, Ju X, Chen H, et al. PSMA-targeted nanoparticles for specific penetration of blood−brain tumor barrier and combined therapy of brain metastases. *J Control Release* 2021;**329**:934−47.

29. Miao TT, Ju XF, Zhu QN, Wang YM, Guo Q, Sun T, et al. Nano-particles surmounting blood−brain tumor barrier through both trans-cellular and paracellular pathways to target brain metastases. *Adv Funct Mater* 2019;**29**:1900259.

30. Guo Q, Zhu Q, Miao T, Tao J, Ju X, Sun Z, et al. LRP1-upregulated nanoparticles for efficiently conquering the blood−brain barrier and targetedly suppressing multifocal and infiltrative brain metastases. *J Control Release* 2019;**303**:117−29.

31. Chen H, Zhou M, Zeng Y, Miao T, Luo H, Tong Y, et al. Biomimetic lipopolysaccharide-free bacterial outer membrane-functionalized nanoparticles for brain-targeted drug delivery. *Adv Sci* 2022;**9**:e2105854.

32. Ju X, Chen H, Miao T, Ni J, Han L. Prodrug delivery using dual-targeting nanoparticles to treat breast cancer brain metastases. *Mol Pharm* 2021;**18**:2694−702.

33. Khan NU, Ni J, Ju X, Miao T, Chen H, Han L. Escape from ablu-minal LRP1-mediated clearance for boosted nanoparticle brain de-livery and brain metastasis treatment. *Acta Pharm Sin B* 2021;**11**:1341−54.

34. Zhou M, Chen H, Zeng Y, Lv Z, Hu X, Tong Y, et al. DH5α outer membrane-coated biomimetic nanocapsules deliver drugs to brain metastases but not normal brain cells *via* targeting GRP94. *Small* 2023;**19**:e2300403.

35. Eichler AF, Chung E, Kodack DP, Loeffler JS, Fukumura D, Jain RK. The biology of brain metastases-translation to new therapies. *Nat Rev Clin Oncol* 2011;**8**:344−56.

36. Liu Z, Wang Y, Kabraji S, Xie S, Pan P, Liu Z, et al. Improving orthotopic mouse models of patient-derived breast cancer brain me-tastases by a modified intracarotid injection method. *Sci Rep* 2019;**9**:622.

37. Ni J, Ramkissoon SH, Xie S, Goel S, Stover DG, Guo H, et al. Combination inhibition of PI3K and mTORC1 yields durable re-missions in mice bearing orthotopic patient-derived xenografts of HER2-positive breast cancer brain metastases. *Nat Med* 2016;**22**:723−6.

38. Oshi M, Okano M, Maiti A, Rashid OM, Saito K, Kono K, et al. Novel breast cancer brain metastasis patient-derived orthotopic xenograft model for preclinical studies. *Cancers* 2020;**12**:444.

39. Linot B, Campone M, Augereau P, Delva R, Abadie-Lacourtoisie S, Nebout-Mesgouez N, et al. Use of liposomal doxorubicin-cyclophosphamide combination in breast cancer patients with brain metastases: a monocentric retrospective study. *J Neuro Oncol* 2014;**117**:253−9.

40. Lu YS, Chen TW, Lin CH, Yeh DC, Tseng LM, Wu PF, et al. Bev-acizumab preconditioning followed by etoposide and cisplatin is highly effective in treating brain metastases of breast cancer pro-gressing from whole-brain radiotherapy. *Clin Cancer Res* 2015;**21**:1851−8.

41. Guo Q, Chang Z, Khan NU, Miao T, Ju X, Feng H, et al. Nanosizing noncrystalline and porous silica material-naturally occurring opal shale for systemic tumor targeting drug delivery. *ACS Appl Mater Interfaces* 2018;**10**:25994−6004.

42. Kheirolomoom A, Kim CW, Seo JW, Kumar S, Son DJ, Gagnon MK, et al. Multifunctional nanoparticles facilitate molecular targeting and miRNA delivery to inhibit atherosclerosis in apoE$^{−/−}$ mice. *ACS Nano* 2015;**9**:8885−97.

43. Yin HJ, Shi XF, Wang H, Jin WD, Li YX, Fu Y. Photodynamic therapy targeting VCAM-1-expressing human umbilical vein endothelial cells using a PpIX-VCAM-1 binding peptide-quantum dot conjugate. *RSC Adv* 2017;**7**:50562−70.

44. Heck AM, Yanovski JA, Calis KA. Orlistat, a new lipase inhibitor for the management of obesity. *Pharmacotherapy* 2000;**20**:270−9.

45. Guerit S, Fidan E, Macas J, Czupalla CJ, Figueiredo R, Vijikumar A, et al. Astrocyte-derived Wnt growth factors are required for endo-thelial blood−brain barrier maintenance. *Prog Neurobiol* 2021;**199**:101937.

46. Nitta T, Hata M, Gotoh S, Seo Y, Sasaki H, Hashimoto N, et al. Size-selective loosening of the blood−brain barrier in claudin-5-deficient mice. *J Cell Biol* 2003;**161**:653−60.

47. Yanagida K, Liu CH, Faraco G, Galvani S, Smith HK, Burg N, et al. Size-selective opening of the blood−brain barrier by targeting endo-thelial sphingosine 1-phosphate receptor 1. *Proc Natl Acad Sci U S A* 2017;**114**:4531−6.

48. Lien EC, Westermark AM, Zhang Y, Yuan C, Li Z, Lau AN, et al. Low glycaemic diets alter lipid metabolism to influence tumour growth. *Nature* 2021;**599**:302−7.

49. Haase D, Schmidl S, Ewald C, Kalff R, Huebner C, Firsching R, et al. Fatty acid synthase as a novel target for meningioma therapy. *Neuro Oncol* 2010;**12**:844−54.

50. Zhao W, Kridel S, Thorburn A, Kooshki M, Little J, Hebbar S, et al. Fatty acid synthase: a novel target for antiglioma therapy. *Br J Cancer* 2006;**95**:869−78.

51. Cheng YJ, Fan F, Zhang Z, Zhang HJ. Lipid metabolism in malignant tumor brain metastasis: reprogramming and therapeutic potential. *Expert Opin Ther Targets* 2023;**27**:861−78.

52. Lippmann ES, Azarin SM, Kay JE, Nessler RA, Wilson HK, Al-Ahmad A, et al. Derivation of blood−brain barrier endothelial cells from human pluripotent stem cells. *Nat Biotechnol* 2012;**30**:783−91.

53. Qian T, Maguire SE, Canfield SG, Bao X, Olson WR, Shusta EV, et al. Directed differentiation of human pluripotent stem cells to blood−brain barrier endothelial cells. *Sci Adv* 2017;**3**:e1701679.

54. McCord M, Mukouyama YS, Gilbert MR, Jackson S. Targeting WNT signaling for multifaceted glioblastoma therapy. *Front Cell Neurosci* 2017;**11**:318.

55. Laksitorini MD, Yathindranath V, Xiong W, Hombach-Klonisch S, Miller DW. Modulation of Wnt/beta-catenin signaling promotes blood−brain barrier phenotype in cultured brain endothelial cells. *Sci Rep* 2019;**9**:19718.

56. Kania KD, Wijesuriya HC, Hladky SB, Barrand MA. Beta amyloid effects on expression of multidrug efflux transporters in brain endothelial cells. *Brain Res* 2011;**1418**:1−11.

57. Akita H, Fujiwara T, Santiwarangkool S, Hossen N, Kajimoto K, El-Sayed A, et al. Transcytosis-targeting peptide: a conductor of liposomal nanoparticles through the endothelial cell barrier. *Small* 2016;**12**:1212−21.

58. Guo S, Som AT, Arai K, Lo EH. Effects of angiotensin-II on brain endothelial cell permeability *via* PPARalpha regulation of para- and trans-cellular pathways. *Brain Res* 2019;**1722**:146353.

59. Patel B, Yang PH, Kim AH. The effect of thermal therapy on the blood−brain barrier and blood−tumor barrier. *Int J Hyperther* 2020;**37**:35−43.

60. Liebner S, Corada M, Bangsow T, Babbage J, Taddei A, Czupalla CJ, et al. Wnt/beta-catenin signaling controls development of the blood−brain barrier. *J Cell Biol* 2008;**183**:409−17.

61. Polakis P. Formation of the blood−brain barrier: Wnt signaling seals the deal. *J Cell Biol* 2008;**183**:371−3.

62. Artus C, Glacial F, Ganeshamoorthy K, Ziegler N, Godet M, Guilbert T, et al. The Wnt/planar cell polarity signaling pathway contributes to the integrity of tight junctions in brain endothelial cells. *J Cerebr Blood Flow Metabol* 2014;**34**:433−40.

63. Harati R, Benech H, Villegier AS, Mabondzo A. P-glycoprotein, breast cancer resistance protein, organic anion transporter 3, and transporting peptide 1a4 during blood−brain barrier maturation: involvement of Wnt/beta-catenin and endothelin-1 signaling. *Mol Pharm* 2013;**10**:1566−80.

64. Drewes LR. Frizzled fissure to improve central nervous system drug delivery? *J Cerebr Blood Flow Metabol* 2014;**34**:1257.

65. Pinzon-Daza ML, Salaroglio IC, Kopecka J, Garzon R, Couraud PO, Ghigo D, et al. The cross-talk between canonical and non-canonical Wnt-dependent pathways regulates P-glycoprotein expression in human blood−brain barrier cells. *J Cerebr Blood Flow Metabol* 2014;**34**:1258−69.

66. Guerit S, Liebner S. Blood−brain barrier breakdown determines differential therapeutic outcome in genetically diverse forms of medulloblastoma. *Cancer Cell* 2016;**29**:427−9.

67. Sidaway P. CNS cancer: Wnt affects blood−brain barrier permeabilty. *Nat Rev Clin Oncol* 2016;**13**:330.

68. Lim JC, Kania KD, Wijesuriya H, Chawla S, Sethi JK, Pulaski L, et al. Activation of beta-catenin signalling by GSK-3 inhibition increases p-glycoprotein expression in brain endothelial cells. *J Neurochem* 2008;**106**:1855−65.

69. Park CH, Chang JY, Hahm ER, Park S, Kim HK, Yang CH. Quercetin, a potent inhibitor against beta-catenin/Tcf signaling in SW480 colon cancer cells. *Biochem Biophys Res Commun* 2005;**328**:227−34.

70. Riganti C, Salaroglio IC, Caldera V, Campia I, Kopecka J, Mellai M, et al. Temozolomide downregulates P-glycoprotein expression in glioblastoma stem cells by interfering with the Wnt3a/glycogen synthase-3 kinase/beta-catenin pathway. *Neuro Oncol* 2013;**15**:1502−17.

71. Han L. Modulation of the blood−brain barrier for drug delivery to brain. *Pharmaceutics* 2021;**13**:2024.

72. Gao X, Qian J, Zheng S, Changyi Y, Zhang J, Ju S, et al. Overcoming the blood−brain barrier for delivering drugs into the brain by using adenosine receptor nanoagonist. *ACS Nano* 2014;**8**:3678−89.

73. Carman AJ, Mills JH, Krenz A, Kim DG, Bynoe MS. Adenosine receptor signaling modulates permeability of the blood−brain barrier. *J Neurosci* 2011;**31**:13272−80.

74. Han L, Kong DK, Zheng MQ, Murikinati S, Ma C, Yuan P, et al. Increased nanoparticle delivery to brain tumors by autocatalytic priming for improved treatment and imaging. *ACS Nano* 2016;**10**:4209−18.

75. Han L, Jiang C. Evolution of blood−brain barrier in brain diseases and related systemic nanoscale brain-targeting drug delivery strategies. *Acta Pharm Sin B* 2021;**11**:2306−25.